

Short Communication

Effect of Heat Energy Input on Electrochemical Properties of Solution-Annealed Super-Duplex Stainless Steel UNS S 32750 Laser Welding

Changwon Sung¹, Byung-Hyun Shin^{2,*}, and Wonsub Chung^{3,*}

¹ Kowel Corporation, Yangsan, Republic of Korea

² Cold Rolling Production Engineering Team, Hyungdai steel, Dangjin-Si 31719, Republic of Korea

³ School of Materials Science and Engineering, Pusan National University, Busan 46241, Republic of Korea

*E-mail: lemonhouse947@nate.com & wschung1@pusan.ac.kr

Received: 2 December 2021 / Accepted: 17 January 2022 / Published: 2 February 2022

Super duplex stainless steel (SDSS) exhibits a high corrosion resistance in seawater because of the combination of austenite and ferrite present. Laser welding breaks the balance between austenite and ferrite owing to changes in the microstructure during the ferritization. Therefore, the corrosion resistance of the weld zone on SDSS depends on the heat energy input. In this study, we examined the electrochemical behavior of SDSS after laser welding at different heat energy inputs. It was observed that laser welding reduced the corrosion resistance of SDSS, which depended on the heat energy input. The corrosion resistance of the surface of welded SDSS was determined by analyzing the open circuit potential, potentiodynamic polarization tests, critical pitting temperature (CPT), and electrochemical impedance spectroscopy. An increase in the heat energy input decreased the corrosion resistance and the thickness of SDSS and the passivation layer, respectively. However, after full penetration, the CPT of SDSS increased from 48 to 61 °C. The electrochemical properties of SDSS was affected by the surface reactivity and shape of the bead.

Keywords: electrochemical properties; laser welding; heat input energy; super-duplex stainless steel; solution annealing

1. INTRODUCTION

The excellent strength and corrosion resistance of stainless steel enables its use as a structural material of offshore plant. Super duplex stainless steel (SDSS), in addition to strength, possesses an excellent corrosion resistance, and thus it can be used as a structural material in seawater. For this reason, the use of SDSS as an offshore structural material has been extensively studied [1-10].

SDSS is used in pipes and valves in offshore plant and structure [3]. Although seamless pipes are primarily used, because of their high prices, research on welding is being needed [11-15]. General pipes are produced using resistance seam welding; however, this cannot be applied to SDSS pipes as they have thicknesses of 25 mm or more [13]. For these pipes, welding methods, namely laser welding and arc welding, are used. Arc welding can be performed in different ways, depending on the pipe conditions. A large amount of heat input energy is required in the process; therefore, a secondary phase is deposited on the weld surface [14]. Laser welding, however, requires a small amount of heat input energy and has a high welding speed [15].

Many studies have been conducted on heat-treatment conditions of SDSS and its physical properties after welding [1-3]. Tan analyzed the corrosion resistance based on phase fractions at different heat-treatment temperatures of SDSS. Shin analyzed electrochemical properties of SDSS at different heat-treatment temperatures and cooling rates [1]. Saravanan analyzed mechanical properties of SDSS after laser welding [15]. Although many studies have been conducted on SDSS, studies on its electrochemical properties according to the amount of heat input energy and the factors affecting it are scarce.

Therefore, in this study, we analyzed the effect of the amount of heat input energy on the structure and electrochemical properties of the SDSS laser weld zone. The microstructure of the weld zone was analyzed using optical microscopy (OM) and field-emission scanning electron microscopy (FE-SEM). The electrochemical properties were examined by analyzing the open circuit potential (OCP), potentiodynamic polarization test, critical pitting temperature (CPT), and electrochemical impedance spectroscopy (EIS).

2. EXPERIMENTAL

The material used in this study was SDSS, classified as 2507. Its chemical composition is shown in Table 1. The pitting resistance equivalent was calculated using $PRE = \text{wt.\% Cr} + 3.3 \text{ wt.\% Mo} + 16 \text{ wt.\% N}$. 42 super grade duplex stainless steel [3].

Table 1. Chemical composition of SDSS UNS S 32750.

| | C | N | Mn | Ni | Cr | Mo | Cu | W | Fe |
|-------------|------|------|-----|-----|------|-----|-----|------|-----|
| UNS S 32750 | 0.01 | 0.27 | 0.8 | 6.8 | 25.0 | 3.8 | 0.2 | 0.02 | Bal |

Table 2. Laser welding conditions of SDSS UNS S 32750.

| Specimen | # 1 | # 2 | # 3 | # 4 | # 5 | # 6 |
|-------------------|------|------|------|------|------|------|
| Welding power, kW | 0.00 | 0.50 | 0.75 | 1.00 | 1.25 | 2.50 |

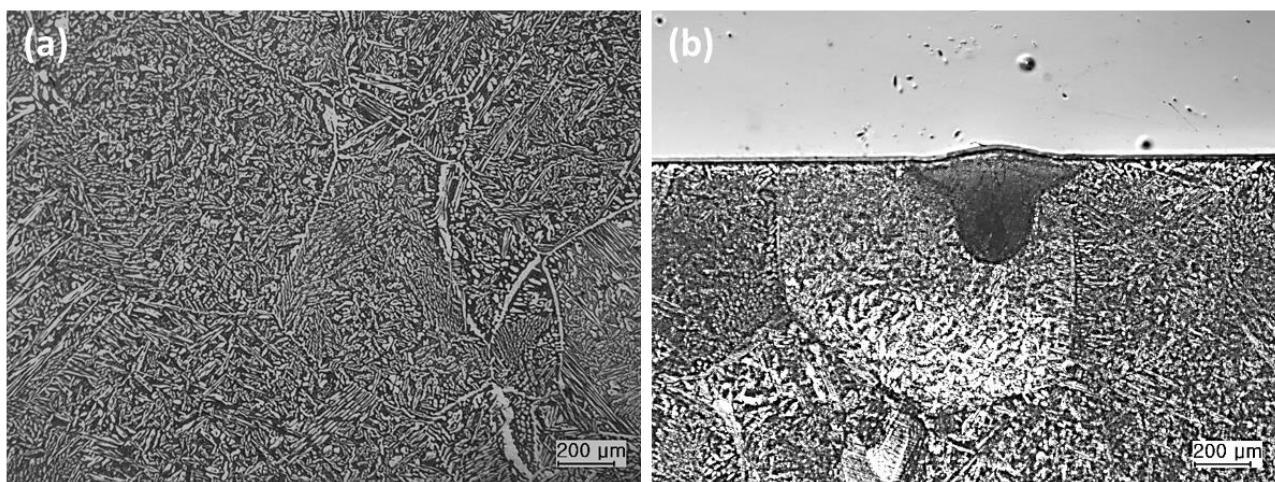
To perform the laser welding of SDSS, 25 mm of SDSS was butt laser welded. Laser welding conditions are listed in Table 2. The surface and cross section microstructures of laser welded SDSS were analyzed. Microstructures on the cross section were analyzed by OM, and those on the surface were analyzed by FE-SEM. After polishing the surface to analyze cross-section microstructures, an electrolytic etching was performed in an electrolyte solution (20 wt.% NaOH). Using the shape of the cross section, the size of the laser weld was measured by the welding bead and depth.

The electrochemical properties of the laser weld zone in SDSS were analyzed in four steps: using a three electrode cell, consisting of a working electrode (WE, specimen), counter electrode (CE, Pt mesh), and reference electrode (RE, saturated calomel electrode (SCE)); analyzing the OCP; performing the potentiometric polarization test; and using EIS in 3.5 wt.% NaCl. The OCP was used to measure the voltage change on the weld surface for 3600 s, which was then used to measure the reactivity of the laser-welded SDSS surface. The potentiodynamic polarization test was performed to measure the change in the current density at a rate of 0.167 mV and a voltage of -0.5 ~ 1.5 V. EIS was used to measure the reactivity of the weld surface from $10 \sim 10^4$ Hz. The CPT was calculated in 5.85 wt. % NaCl at 700 mV, and it was determined as the temperature over $100 \mu\text{A}/\text{cm}^2$ for 60 s at a scan rate of $1 \text{ }^\circ\text{C}/\text{min}$.

3. RESULTS AND DISCUSSION

3.1. Microstructure and morphology of laser welded SDSS

In laser welding, the morphology of the weld zone changes depending on the amount of heat energy input [13-15]. Fig. 1 shows cross sectional images of the laser weld zone at different heat input energy [14]. The laser welded microstructure was a ferrite, while the heat affected zone (HAZ) could not be identified because low heat input energy can't make the transformation of phase [13, 15, 16]. Arc welding forms secondary phases, such as CrN, whereas laser welding does not, owing to its low heat input energy.



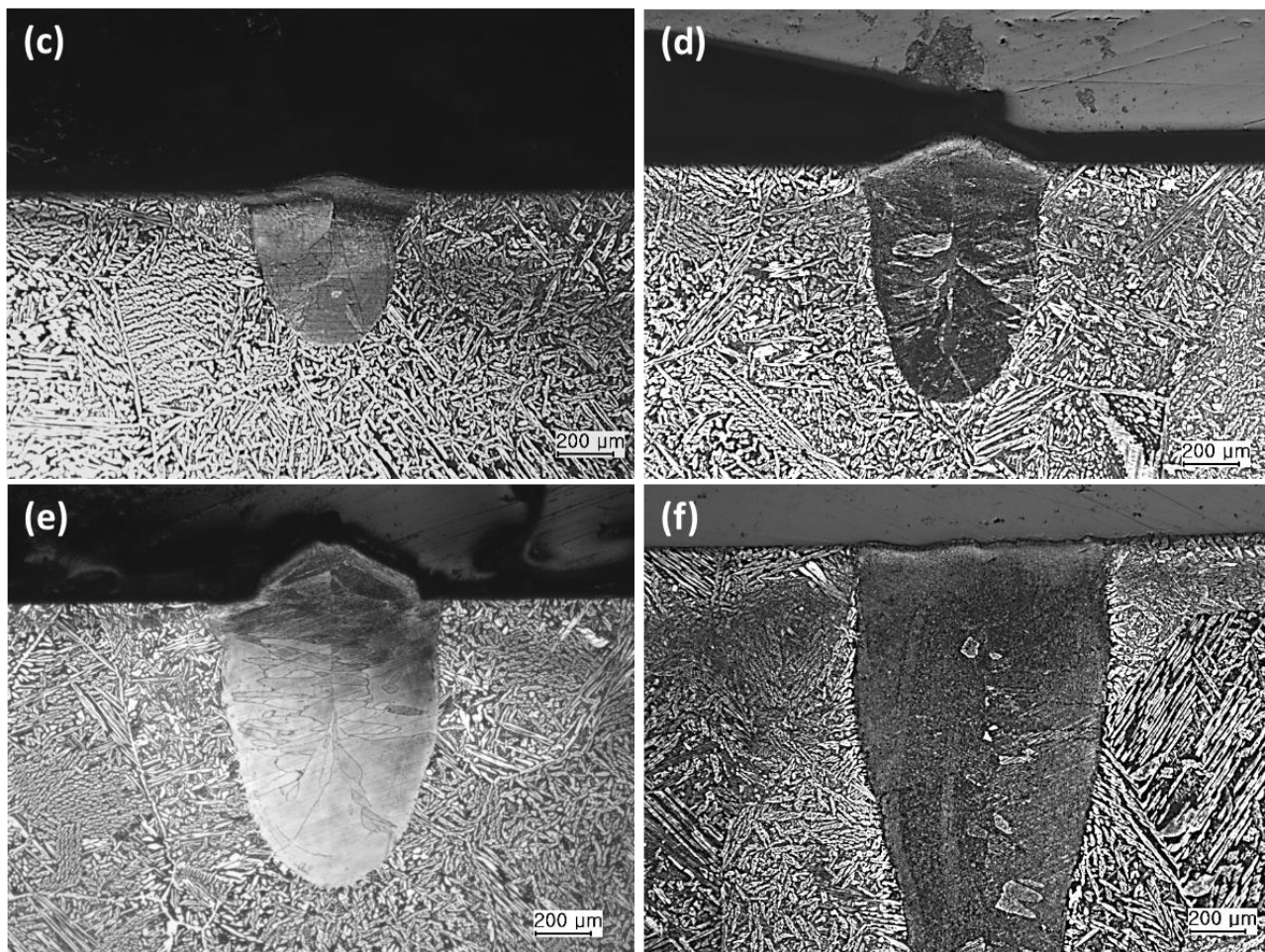


Figure 1. Cross-sectional image of SDSS UNS S 32750 laser-welded at different welding powers: (a) 0.00, (b) 0.25, (c) 0.5, (d) 0.75, (e) 1.00, and (f) 2.50 kW.

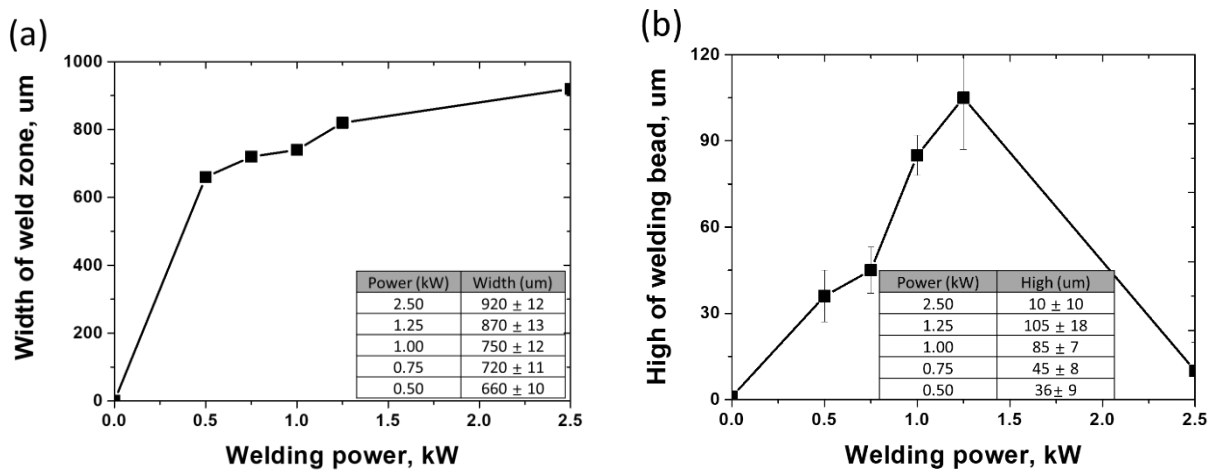


Figure 2. Width of the weld zone and the height of the welding bead in SDSS UNS S 32750 as functions of the laser welding power (kW).

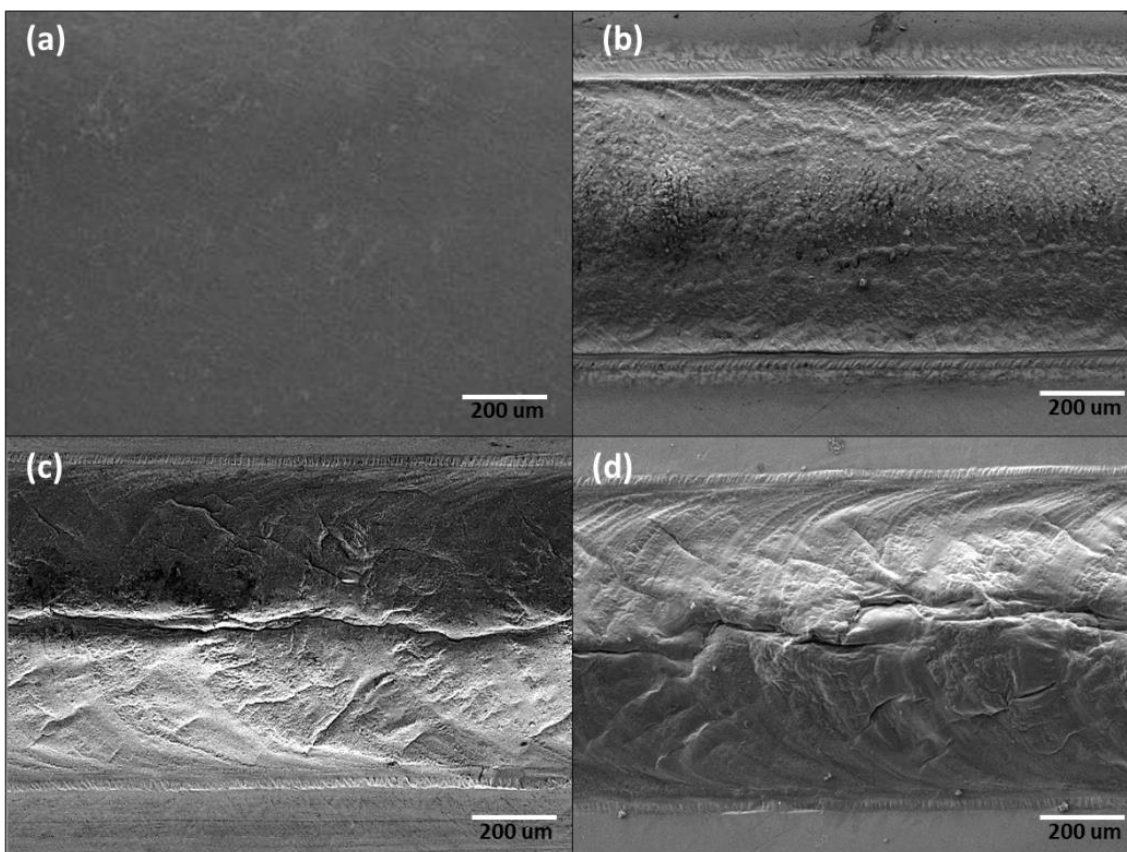


Figure 3. Surface microstructure of laser-welded SDSS UNS S 32750: (a) 0.00, (b) 0.25, (c) 1.25, and (d) 2.50 kW.

As the laser welding heat input energy increases, the laser welding bead and width increase and that show Fig. 2. However, after full penetration, the weld bead decreases significantly (to 10 μm) and is lower than that at 0.5 kW (36 μm). The laser welding bead becomes less uniform as the heat input energy increases, as shown in Fig. 3. No surface cracks were observed at a heat energy input of 0.5 kW, and the welding history and seam marks on the surface were evident afterwards.

Laser welding does not form a secondary phase, even if the heat input energy is increased. If the secondary phase does not form, the corrosion resistance should not decrease because of a chemical composition change. However, the increase in the welding bead size affects the corrosion resistance as it changes the surface area.

3.2. Electrochemical properties of laser welded SDSS

The electromotive force (EMF) series shows the reactivity of materials but is only applicable to pure metals; furthermore, the corrosion resistances of segregated microstructures, such as laser welds, cannot be calculated using the EMF series. Therefore, OCP was used. As the heat input energy increases, the reactivity of laser welded SDSS increases, as shown in Fig. 4. Increases in the ferritization and the weld size acted as factors to reduce the corrosion resistance of SDSS.

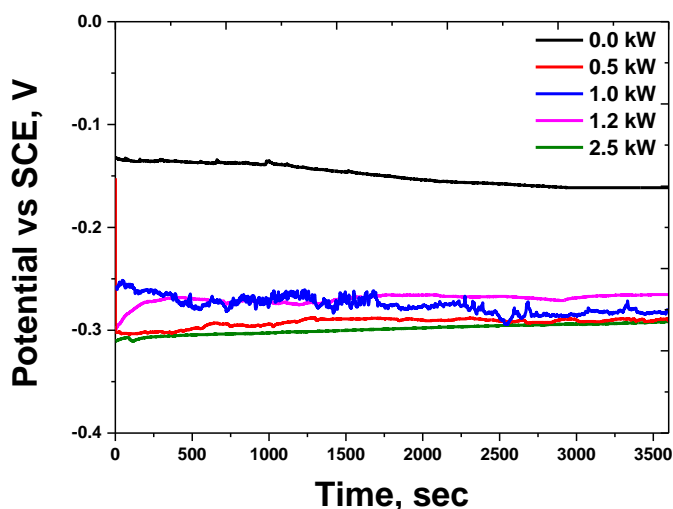


Figure 4. OCP curve (potential with time) in a 3.5 wt.% NaCl electrolyte of SDSS UNS S 32750 samples welded at different welding powers.

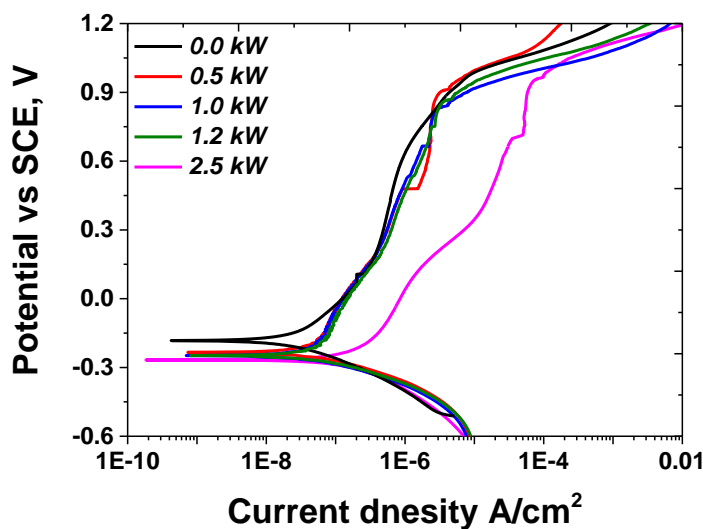


Figure 5. Potentiodynamic polarization curve (current density change with potential vs. SCE) in a 3.5 wt.% NaCl electrolyte of SDSS UNS S 32750 samples welded at different welding powers.

The results of potentiodynamic polarization test showed in Fig. 5 and Table 3 [1, 3]. After laser welding, the reactivity (E_{corr}) at the active polarization curve decreased, and the corrosion rate (I_{corr}) increased. The pitting potential (E_{pit}) in low heat input energy decreased but was restored after full penetration. After full penetration, the rate of uniform corrosion increased owing to the ferrite area increase, but the pitting potential decreased owing to the surface area decrease.

Table 3. Values of major points (E_{corr} , I_{corr} , and E_{pit}) on the potentiodynamic polarization curve of laser-welded SDSS UNS S32750.

| Welding power | E_{corr} | I_{corr} | E_{pit} |
|---------------|------------|-----------------------------------|-----------|
| Bare metal | - 160 mV | $2 \times 10^{-7} \text{ A/cm}^2$ | 990 mV |
| 0.5 kW | - 250 mV | $4 \times 10^{-7} \text{ A/cm}^2$ | 920 mV |
| 1.0 kW | - 270 mV | $4 \times 10^{-7} \text{ A/cm}^2$ | 890 mV |
| 1.2 kW | - 270 mV | $4 \times 10^{-7} \text{ A/cm}^2$ | 900 mV |
| 2.5 kW | - 280 mV | $3 \times 10^{-6} \text{ A/cm}^2$ | 970 mV |

The CPT was used to evaluate the pitting corrosion resistance of duplex stainless steel (DSS) [1]. Fig. 6 shows a plot of the CPT against the heat energy input. Although the corrosion resistance is restored after full penetration, the CPT of the welded material is lower than that of the base material before welding, even though the material areas are the same. Ferritization reduces the pitting corrosion resistance of SDSS to a level of that of standard DSS ($30 < PRE < 40$).

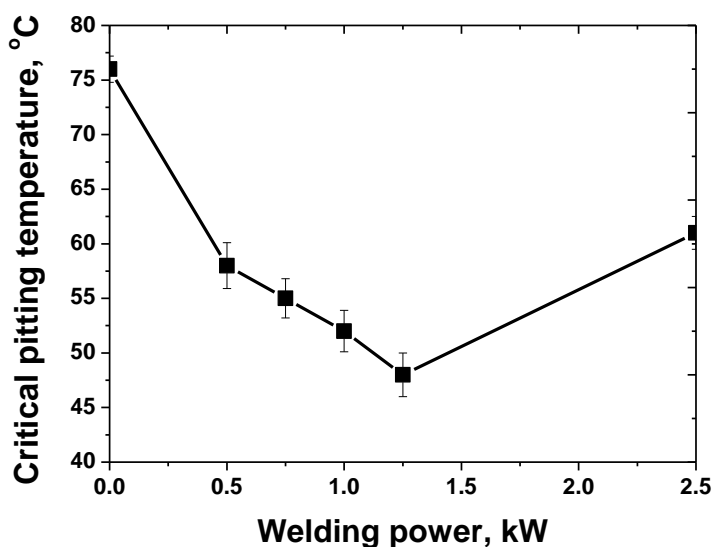


Figure 6. CPT in a 5.85 wt.% NaCl electrolyte of SDSS UNS S 32750 samples welded at different welding powers.

EIS can be used to predict the state of the passivation layer by measuring the surface reactivity [1, 17, 18]. EIS results are shown in Fig. 7. As the heat energy input increases, the resistance of the surface decreases, indicating a decrease in the passivation layer. The passivation layer is very important in SDSS because it evidences the corrosion resistance of stainless steel.

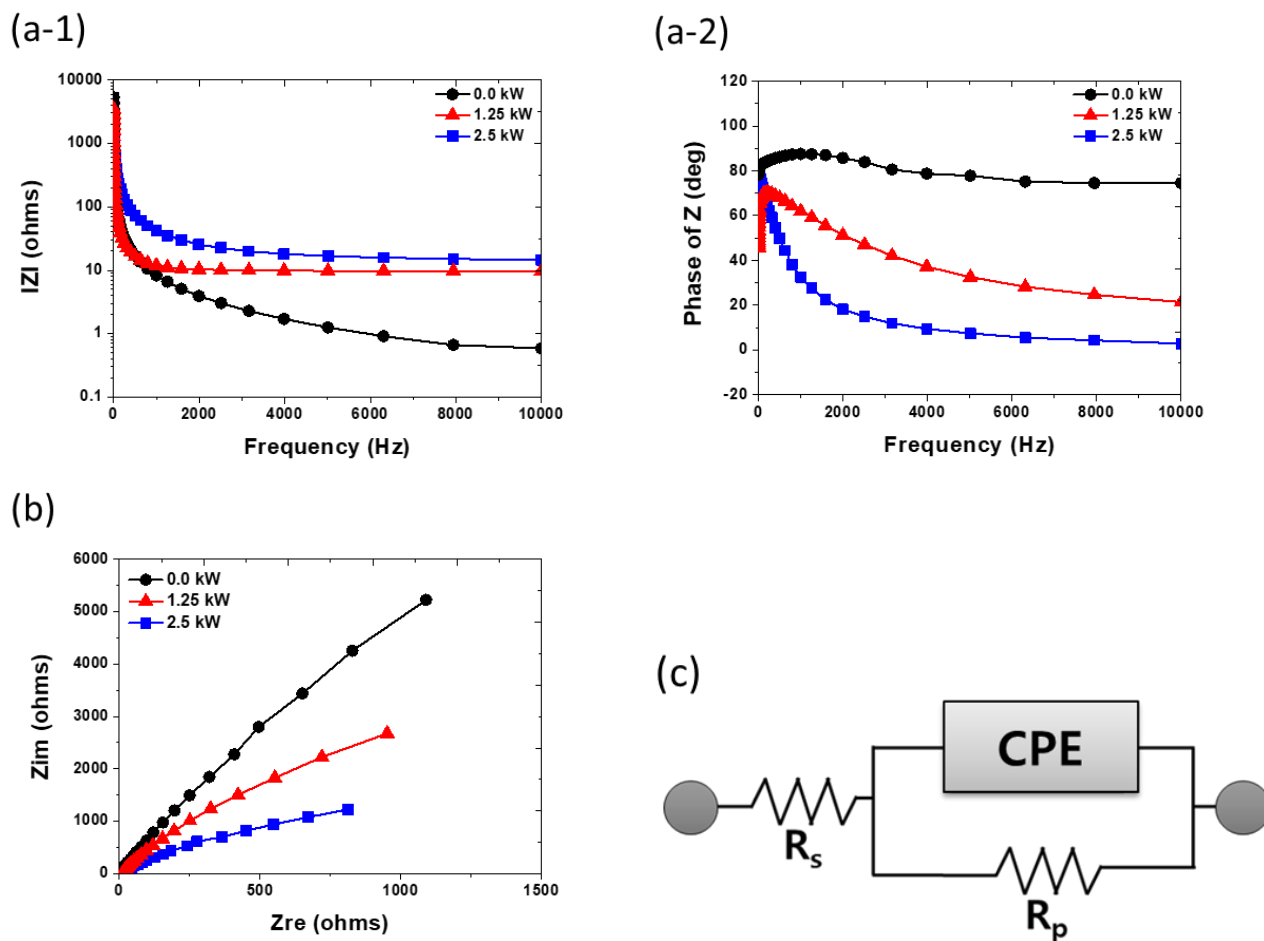


Figure 7. (a) Bode diagrams of SDSS UNS S32750 in a 3.5 wt.% NaCl solution: (a-1) IZI as a function of the frequency (Ohms), (a-2) Phase of Z (Ohms) as a function of the frequency, (b) Nyquist diagram of laser-welded SDSS UNS S32750 in a 3.5 wt.% NaCl solution, and (c) Electrical equivalent circuit used to fit the Bode phase diagrams of SDSS UNS S 32750.

Analyses of the microstructure and electrochemical properties showed that the corrosion resistance against uniform corrosion and the pitting corrosion resistance of SDSS decreased after laser welding [13]. After full penetration, the passivation layer of the SDSS decreased, but the corrosion resistance was recovered because of the decrease in the welded surface area [18]. Laser welding of SDSS reduced the CPT to 47 °C owing to the ferritization; however, it could be restored to 60 °C by removing the welding bead [12-14]. The pitting corrosion resistance of SDSS is affected by the microstructure, but its decrease can be prevented by controlling the surface area.

4. CONCLUSIONS

The microstructure (analyzed using OM and FE-SEM) and electrochemical properties (analyzed using the OCP, potential polarization test, CPT, and EIS) of SDSS, UNS S 32750, were investigated after laser welding, and following conclusions were drawn:

- 1) The laser weld zone of SDSS had a ferrite microstructure. The surface area changed as a function of the heat energy input, and the change in the bead was greater than the change in the width. Also, the laser weld zone did not contain a heat affected zone, and the absence of the secondary phase was confirmed.
- 2) The reactivity (OCP, E_{corr}) of laser welded SDSS decreased owing to the ferritization. This was attributed to the reduction in the passivation layer (shown by EIS) of the surface. However, even though the passivation layer decreased with the increase in the heat energy input, the pitting corrosion resistance of SDSS was restored because of the surface area decrease.
- 3) As SDSS laser welds do not form secondary phases or heat-affected zones, the pitting corrosion resistance of laser-welded SDSS depends on the surface area. The surface area of the weld was most affected by the weld bead—if a post-treatment is not performed after laser welding, the corrosion resistance of SDSS can be improved through a full penetration.

ACKNOWLEDGMENTS

This study was supported by a National Research Foundation of Korea (NRF) grant (no. 2020R1A5A8018822) funded by the Korean Government (MSIT).

References

1. B. H. Shin, J. Park, J. Jeon, S. Heo, and W. Chung, *Anti-Corros. Methods mater.*, 65 (2018) 492.
2. J. Kim, S. Choi, D. Park, and J. Lee, *Mater Des.*, 65 (2015) 914.
3. J. Jang, J. Ju, B. Lee, D. Kwon, and S. Kim, *Mater Sci Eng A.*, 340, 1–2 (2003) 68.
4. J. O. Nilsson, *J. Mater. Sci. Technol.*, 8 (1992) 685.
5. J. M. Pardal, S. S. M. Tavares, M. C. Fonseca, J. A. de Souza, R. R. A. Corte, and H. F. G. de Abreu, *Mater. Charact.*, 60 (2009) 165.
6. T. H. Chen, and J. R. Yang, *Mat. Sci. Eng. A-Struct.*, 311 (2001) 28.
7. C. J. Park, V. S. Rao, and H. S. Kwon, *Corrosion.*, 61 (2005) 76.
8. F. Iacoviello, F. Casari, and S. Gialanella, *Corros. Sci.*, 47 (2005) 909.
9. T. H. Chen, K. L. Weng, and J. R. Yan, *Mat. Sci. Eng. A-Struct.*, 338 (2002) 259.
10. M. Pohl, O. Storz, and T. Glogowski, *Mater. Charact.*, 58 (2007) 65.
11. H. Tan, Y. Jiang, B. Deng, T. Sun, and J. Xu, J. Li, *Mater. Charact.*, 60 (2009) 1049.
12. Y. Sato, T. Nelson, C. Sterling, R. Steel, C. Pettersson, *Mater. Sci.*, 397 (2005) 376.
13. B. H. Shin, D. Kim, S. Park, J. Park, M. Hwang, and W. Chung, *Anti-Corros. Methods mater.*, 66, 1 (2019) 61.
14. E. Taban, E. Kaluc, *Weld World.*, 55 (2017) 48.
15. S. Saravanana, K. Raghukandan, N. Sivagurumanikandan, *Mater. Manuf. Process.*, 25 (2017) 284.
16. C. P. Dias, and O. Balancin, *Metal. Mater. Trans., A*, 62 (2016) 155.
17. M. Martins, and L. C. Casteletti, *Mater. Charact.*, 60 (2009) 150.
18. E. Angelini, B. D. Benedetti, and F. Rosalbino, *Corros. Sci.*, 46 (2004) 1351.